Apparent Radius of Gyration of Diblock Copolymers

William E. McMullen*

Department of Chemistry, Texas A&M University, College Station, Texas 77843

Karl F. Freed and Binny J. Cherayil†

The James Franck Institute and the Department of Chemistry, The University of Chicago, Chicago, Illinois 60637. *Received June 16, 1988*

ABSTRACT: Renormalization group methods are used to determine expressions for the apparent radius of gyration and block expansion factors of an AB diblock chain in dilute solution as functions of the three independent excluded-volume parameters, the two block lengths and the blocks' refractive-index increments. We exploit certain symmetry and topological relations between terms in the perturbation series of the internal vector distribution function to simplify the evaluation of the apparent radius of gyration to order $\epsilon = 4 - d$. This calculation also provides equations for the block expansion factors that describe the effect of AB heterocontacts on the size of the separate blocks relative to their precursor homopolymers. After making our expressions consistent with the known scaling limits of the diblock chain, we compare the theoretical predictions to Monte Carlo simulations and find good agreement. The final equations are applicable to the complete range of solvent and temperature conditions, between and including the Θ- and good-solvent limits.

I. Introduction

Theories[1-4] of dilute and semidilute solution equilibrium properties of homopolymers are well established. Expressions have been determined for homopolymer radii of gyration,[5] second-virial coefficients,[6] mean-square end-vector distances,[7] and even dynamical properties by using renormalization group techniques in conjunction with Edwards' continuum chain representation.[8] This methodology appears capable of well representing all long-wavelength equilibrium properties in terms of the traditional two-parameter[9] model. The theory of transport quantities (e.g., the intrinsic viscosity[10]) and more general nonequilibrium properties[9,11] of dilute solution polymers is less developed; complete results are only available to lowest order in perturbation theory or for approximate models.

The large number of relevant interaction parameters for block copolymers drastically complicates both their experimental[12] and theoretical[13] analysis. Even the simplest case—a diblock copolymer—requires three parameters that vary independently with solvent and temperature to describe the excluded-volume interactions. This makes brute force application of the usual homopolymer theoretical techniques rather complicated. The lack of previous calculations for measurable block copolymer properties is unfortunate in view of the large number of experiments and Monte Carlo simulations[12] performed for such systems. Furthermore, the technological importance[15] of block copolymers motivates a need for accurate methods to characterize them.

Except for a calculation[14] of the second-virial coefficient and, in special limits, the radius of gyration of diblock chains,[13] accurate theoretical calculations of *experimentally* measurable block copolymer properties have not, until now, appeared in the literature. The results outlined in the present paper for the radius of gyration and block expansion factors are much easier to compare to experiment because our formulation of these observables is made by considering dimensionless reduced ratios of different block properties or ratios between block and homopolymer properties[13] for the same solvent conditions and temperature.

One of the most important, experimentally measurable dilute-solution homopolymer properties is the radius of gyration $\langle S^2 \rangle$, generally determined from light-scattering[12,16] experiments. The same experimental appraoch applied to block copolymers only provides an apparent radius of gyration because the intensity of light scattered depends on the (generally different) refractive-index increments of the blocks relative to the solvent. Experiments attempting to address this problem by use of index-matched solvents have encountered the additional difficulty that changing the solvent type alters the values of all three excluded-volume parameters and that perfect index matching is rather rare, so nonnegligible corrections are often required. Furthermore, most experiments[12] to date have been performed on polydisperse block copolymer samples. These complexities have rendered the interpretation of the light-scattering results extremely difficult, and it has not yet been possible to unambiguously assign an actual radius of gyration to the block copolymer chains.

The derivation of a theoretical expression for the *apparent* radius of gyration $\langle S^2 \rangle_{app}$ of a block copolymer in dilute solution can be used straightforwardly to address such complications. The expressions may be averaged over the polymer molecular weight distribution, and the different refractive index increments of the blocks can be used to predict $\langle S^2 \rangle_{app}$. Two of the excluded-volume parameters are readily deduced from homopolymer properties in the same solvent at the same temperature, leaving only a dependence on the third, generally unknown, interblock interaction parameter. The determination of the latter quantity has been the object of many of the previous experiments on block copolymers.[12]

Fröelich and Benoit[17] have calculated the radius of gyration of AB diblocks, and others[18-20] have evaluated the second-virial coefficients of di- and triblock polymers and polymer mixtures using two-parameter (TP) model perturbative calculations. These results are only useful in the neighborhood of an idealized block copolymer Θ state where all three excluded-volume parameters vanish simultaneously. For any given diblock copolymer, it is unlikely that such a solvent and temperature combination exists.[13] Hence, the TP results are, by themselves, of little practical utility. Douglas and Freed[13] have applied RG methods to block copolymers with explicit calculations for the mean-square end-vector distance and some block radii of gyration. The latter are considered only in the special limit of the blocks in a common Θ solvent with equal refractive index increments. They compare their predictions for these quantities to Monte Carlo calculations.[12] The derivations and discussion presented below supplement their analysis by extending the theory to experimentally realizable diblock copolymer systems (which generally in-

† Present address: Baker Laboratory, Cornell University, Ithaca, NY 14583.

0024-9297/89/2222-1853$01.50/0

volve blocks of different lengths and refractive-index increments) and therefore enable the comparison of theory to the $\langle S^2\rangle_{app}$ measured in light scattering experiments.

The present paper uses the TP model in conjunction with RG techniques to derive expressions for the apparent radius of gyration of a diblock copolymer as a function of solvent quality for individual blocks, their interactions, temperature, and the refrctive-index increments. We perform first-order perturbation calculations in ϵ ($\epsilon = 4 - d$, where d is the dimensionality) for the apparent radius of gyration as a function of both refractive-index increments and the three excluded-volume parameters. Block copolymer properties are expressed in terms of similar homopolymer ones under the same solvent and temperature conditions. This produces universal ratios characterizing the block copolymer properties. Either experimental values of higher order theoretical expressions may be used for the homopolymer quantities. We test the adequacy of our first-order approximations for the universal ratio by comparing them to Monte Carlo simulation data of Tanaka and co-workers,[12] extending the previous comparisons[13] that are made for special limits.

The derivation of the diblock radius of gyration and block expansion factors is outlined in section II. Dimensionless ratios are formed between the radii of gyration of the individual blocks and those of homopolymers of the same size. After making the results consistent with the known scaling limits of diblock chains, we introduce a set of TP-like variables,[14] $\bar{z}_A$, $\bar{z}_B$, and $\bar{z}_{AB}$, to describe the crossover from the weakly interacting Θ region ($\bar{z}_A$, $\bar{z}_B$, and $\bar{z}_{AB} \to 0$) to the strongly interacting good-solvent one, where $\bar{z}_A$, $\bar{z}_B$, and $\bar{z}_{AB} > 1$. Section III presents a comparison of the theory, developed in section II to the Monte Carlo simulations. An Appendix elaborates on some of the mathematical details of section II.

II. Theory

A. Diblock Copolymer Model. We consider an infinitely dilute solution of AB diblock copolymers. The interactions between A (B) monomers are modeled[2] in terms of a bare excluded volume interaction parameter v_A^0 (v_B^0). Likewise, v_{AB}^0 describes the interaction between A–B segments. The unperturbed (bare) length of the A block is N_A^0 and that of the B block is N_B^0. Superscript zeros indicate bare quantities which are later renormalized to make the final equations independent of irrelevant microscopic, short-wavelength details of the model.

The spatial positions of segments along the polymer backbone are given by $\mathbf{r}_A(\tau_A)$ and $\mathbf{r}_B(\tau_B)$ on the A and B blocks, respectively, where τ_A (τ_B) measures the contour distance of the segment along the chain. It proves convenient to multiply τ_A and τ_B by the Kuhn lengths, l_A and l_B, of the unperturbed blocks and scale the spatial coordinates by $d^{1/2}$, d being the dimensionality. The Edwards-style model continuum Hamiltonian[21] for the diblock copolymer is

$$H[\mathbf{c}_A,\mathbf{c}_B] = \frac{1}{2}\int_0^{N_A^0 l_A} d\tau_A \left[\frac{d\mathbf{C}_A}{d\tau_A}\right]^2 + \frac{1}{2}\int_0^{N_B^0 l_B} d\tau_B \left[\frac{d\mathbf{c}_B}{d\tau_B}\right]^2 + (2\pi)^2\frac{v_A^0}{2}\int_0^{N_A^0 l_A} d\tau_A \int_0^{N_A^0 l_A} d\tau'_A\, \delta[\mathbf{c}_A(\tau_A) - \mathbf{c}_A(\tau'_A)] + (2\pi)^2 v_{AB}^0 \int_0^{N_A^0 l_A} d\tau_A \int_0^{N_B^0 l_B} d\tau_B\, \delta[\mathbf{c}_A(\tau_A) - \mathbf{c}_B(\tau_B)] + (2\pi)^2\frac{v_B^0}{2}\int_0^{N_B^0 l_B} d\tau_B \int_0^{N_B^0 l_B} d\tau'_B\, \delta[\mathbf{c}_B(\tau_B) - \mathbf{c}_B(\tau'_B)] \quad (1)$$

where

$$\mathbf{c}_A = d^{1/2}\mathbf{r}_A \quad (2a)$$

and

$$\mathbf{c}_B = d^{1/2}\mathbf{r}_B \quad (2b)$$

The factors of $(2\pi)^2$ in the nonideal parts of eq 1 make the final equations simpler. We ignore the dependence of the bare interaction parameters in (1) on l_A and l_B as the former are phenomenological (nonuniversal) quantities to be inferred from comparisons with experiment.

The bare internal-vector distribution function $G^0(\mathbf{c}_{21};\tau_2,\tau_1)$ specifies the probability that monomer segments at points τ_2 and τ_1 are separated by $\mathbf{c}_{21}$ ($=\mathbf{c}_2 - \mathbf{c}_1$). The bare radius of gyration is expressed in terms of $G^0(\mathbf{c}_{21};\tau_2,\tau_1)$ by

$$\langle S^2\rangle^0 = -(1/2d)\int_0^{N_A^0 l_A + N_B^0 l_B} d\tau_1 \int_0^{N_A^0 l_A + N_B^0 l_B} d\tau_2 \int d\mathbf{c}_{21}\, |\mathbf{c}_{21}|^2 G^0(\mathbf{c}_{21},\tau_2,\tau_1)\Big[\int_0^{N_A^0 l_A + N_B^0 l_B} d\tau_1 \int^{N_A^0 l_A + N_B^0 l_B} d\tau_2 \int d\mathbf{c}_{21}\, G^0(\mathbf{c}_{21};\tau_2,\tau_1)\Big]^{-1} \quad (3)$$

In the continuum approach $G^0(\mathbf{c}_{21};\tau_2,\tau_1)$ is determined from the path integral

$$G^0(\mathbf{c}_{21};\tau_2,\tau_1) = \int D[\mathbf{c}_A(\tau_A),\mathbf{c}_B(\tau_B)]\delta[\mathbf{c}_2 - \mathbf{c}_1(\tau_2)]\delta[\mathbf{c}_1 - \mathbf{c}_1(\tau_1)]\exp(-H) \quad (4)$$

where τ_2 and τ_1 denote positions along either of the blocks.

Substituting eq 1 and 4 into eq 3 and expanding to first order in the interaction parameters, we find

$$\langle S^2\rangle^0 = -\frac{1}{2d}\frac{\hat{G}_I^{0\prime\prime}(N_A^0,N_B^0)}{\hat{G}_I^0(N_A^0,N_B^0)}\Bigg\{1 - (2\pi)^2 v_A^0\left[\frac{\delta\hat{G}_A^{0\prime\prime}(N_A^0,N_B^0)}{\hat{G}_I^{0\prime\prime}(N_A^0,N_B^0)} - \frac{\delta\hat{G}_A^0(N_A^0,N_B^0)}{\hat{G}_I^0(N_A^0,N_B^0)}\right] - (2\pi)^2 v_{AB}^0\left[\frac{\delta\hat{G}_{AB}^{0\prime\prime}(N_A^0,N_B^0)}{\hat{G}_I^{0\prime\prime}(N_A^0,N_B^0)} - \frac{\delta\hat{G}_{AB}^0(N_A^0,N_B^0)}{\hat{G}_I^0(N_A^0,N_B^0)}\right] - (2\pi)^2 v_B^0\left[\frac{\delta\hat{G}_B^{0\prime\prime}(N_A^0,N_B^0)}{\hat{G}_I^{0\prime\prime}(N_A^0,N_B^0)} - \frac{\delta\hat{G}_B^0(N_A,N_B^0)}{\hat{G}_I^0(N_A^0,N_B^0)}\right]\Bigg\} + O(v_A^{0\,2},v_B^{0\,2},v_A^0 v_B^0,v_{AB}^{0\,2},v_A^0 v_{AB}^0,v_B^0 v_{AB}^0) \quad (5)$$

where the subscript I indicates ideal Gaussian chain quantities, carets designate Fourier transforms with respect to $\mathbf{c}_{21}$, and double primes denote the second derivatives of the Fourier-transformed variables evaluated at $\mathbf{k} = 0$; i.e.

$$\hat{f}(N_A^0,N_B^0) = \hat{f}(\mathbf{k}=0;N_A^0,N_B^0) = \Big[\int d\mathbf{c}_{21}\exp(i\mathbf{k}\cdot\mathbf{c}_{21})f(\mathbf{c}_{21};N_A^0,N_B^0)\Big]_{\mathbf{k}=0} \quad (6a)$$

and

$$\hat{f}''(N_A^0,N_B^0) = \left[\sum_{i=1}^{d}\frac{\partial^2}{\partial k_i^2}\hat{f}(\mathbf{k};N_A^0,N_B^0)\right]_{\mathbf{k}=0} \quad (6b)$$

The quantities $\delta G_A^0(\mathbf{c}_{21};N_A^0,N_B^0)$, $\delta G_B^0(\mathbf{c}_{21};N_A^0,N_B^0)$, and $\delta G_{AB}^0(\mathbf{c}_{21};N_A^0,N_B^0)$ are the coefficients of v_A^0, v_B^0, and v_{AB}^0, respectively, in the first-order perturbation expansion for $G^0(\mathbf{c}_{21};N_A^0,N_B^0)$. Each of these coefficients consists of a number of terms which can be represented diagrammatically. Figure 1 lists the diagrams associated with the ideal terms and those associated with the excluded-volume corrections $\delta G_A^0(\mathbf{c}_{21};N_A^0,N_B^0)$ and $\delta G_{AB}^0(\mathbf{c}_{21};N_A^0,N_B^0)$. The

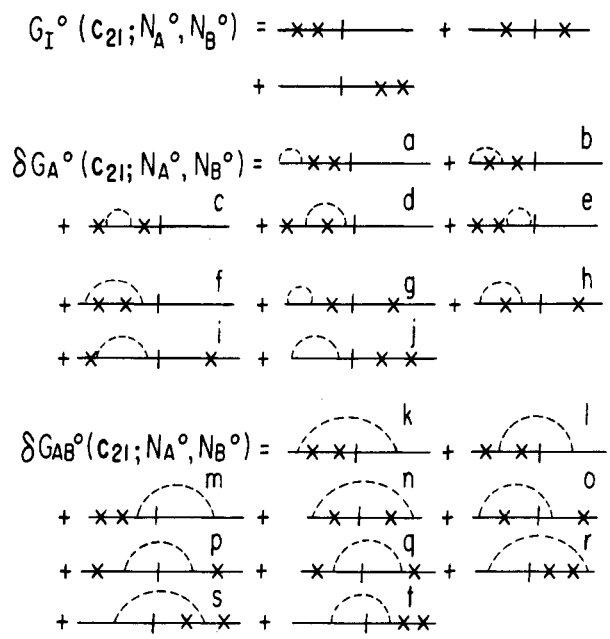

Figure 1. Diagrams in the first-order perturbation series of the internal vector distribution function. The B diagrams, symmetric to the A set, are not shown.

quantity $\delta G_B^0(\mathbf{c}_{21};N_A^0,N_B^0)$ is obtained from $\delta G_A^0(\mathbf{c}_{21};N_A^0,N_B^0)$ by interchanging N_A^0 and N_B^0.

The rules for interpreting these diagrams are as follows: the segments of the diagrams to the left of the center vertical bar correspond to the A block, while those components to the right of the bar describe the B part of the chain. The ×'s denote $\mathbf{c}_2$ and $\mathbf{c}_1$, and the × associated with $\mathbf{c}_2$ always lies to the right of that for $\mathbf{c}_1$. Dashed semicircles indicate the δ-function pseudopotential. Between markings on the diagrams, successive points along the backbone are distributed according to[2]

$$G_I^0(\mathbf{c}_\beta-\mathbf{c}_\alpha;\tau_\beta-\tau_\alpha) = \left[\frac{1}{2\pi|\tau_\beta-\tau_\alpha|}\right]^{d/2}\exp\left\{-\frac{|\mathbf{c}_\beta-\mathbf{c}_\alpha|^2}{2(\tau_\beta-\tau_\alpha)}\right\} \tag{7}$$

where $\mathbf{c}_\beta$ and $\mathbf{c}_\alpha$ denote the position vectors of the markings (×'s, the vertical bar, etc.) and τ_β and τ_α their contour points (i.e., positions on the backbone). For use in the computations described in the appendicies, we provide the Fourier–Laplace transform of eq 7:

$$\hat{G}_I^0(\mathbf{k};s) = (s + k^2/2)^{-1} \tag{8}$$

In the diagrams, it is understood that d-dimensional spatial integrations are performed over the positions of the ends of the blocks (the ends of the diagrams and the center bar) and the points where the dashed lines meet the backbone. We also integrate over the contour points associated with the ×'s and the ends of the semicircles. For example, diagram o of the AB distribution function has the value

$$\begin{aligned}AB_o(\mathbf{c}_{21};N_A^0,N_B^0) = {} & \int d\mathbf{c}(0)\int d\mathbf{c}_A(N_A^0)\int d\mathbf{c}_B(N_B^0)\\ & \int_0^{N_A^0 l_A} d\tau_1 \int_0^{N_B^0 l_B} d\tau_2 \int_0^{\tau_1} d\tau_A\\ & \int_0^{\tau_2} d\tau_B \int d\bar{\mathbf{c}}_1 \int d\bar{\mathbf{c}}_2\, \delta[\bar{\mathbf{c}}_2-\bar{\mathbf{c}}_1]\times\\ & G_I^0(\bar{\mathbf{c}}_1-\mathbf{c}(0);\tau_1)G_I^0(\mathbf{c}_1-\bar{\mathbf{c}}_1;\tau_1-\tau_A)\times\\ & G_I^0(\mathbf{c}(N_A^0)-\mathbf{c}_1;N_A^0-\tau_1)G_I^0(\bar{\mathbf{c}}_2-\mathbf{c}(N_A^0);\tau_B)\times\\ & G_I^0(\mathbf{c}_2-\bar{\mathbf{c}}_2;\tau_2-\tau_B)G_I^0(\mathbf{c}(N_B^0)-\mathbf{c}_2;N_B^0-\tau_2)\end{aligned} \tag{9}$$

In general, the intensity of light scattered from a particular position of the chain varies with its refractive-index increment, λ. Hence, each diagram is weighted by the factor $\lambda_i\lambda_j$, the indices referring to the locations (A or B block) of the ×'s on the diagram. Appendix B outlines the calculation of some of the more complicated diagrams by using Fourier–Laplace methods.

B. Case of Equal Refractive Index Increments and Simplification of Algebra. When $\lambda_A = \lambda_B$ and $v_A^0 = v_B^0 = v_{AB}^0$, the properties of the chain become that of a homopolymer with overall contour length $N_A^0 l_A + N_B^0 l_B$. This simple limit is quite useful for introducing methods of simplifying the determination of the diblock properties.

The first-order perturbation expansion of any dilute solution diblock copolymer property consists of four terms. Besides the ideal contribution, these include the AA, BB, and AB intrachain terms. If we represent the bare property of interest by $P^0(v_A^0,v_B^0,v_{AB}^0,N_A^0,N_B^0)$, to first order we have

$$\begin{aligned}P^0 = {} & P_I^0(N_A^0,N_B^0) + v_A^0 P_A^0(N_A^0,N_B) +\\ & v_B^0 P_B^0(N_A^0,N_B^0) + v_{AB}^0 P_{AB}^0(N_A^0,N_B^0)\end{aligned} \tag{10}$$

In the limit $v_A^0, v_B^0, v_{AB}^0 \to v^0$, P^0 reduces to the homopolymer case which we denote by P_H^0. Equation 10 implies that

$$\begin{aligned}v^0 P_{AB}^0(N_A^0,N_B^0) = {} & \{P_H^0(N_A^0,N_B^0,v^0) - P_I^0(N_A^0,N_B^0) -\\ & v^0[P_A^0(N_A^0,N_B^0) + P_B^0(N_A^0,N_B^0)]\}\end{aligned} \tag{11}$$

Thus, provided P_H^0, P_I^0, P_A^0, and P_B^0 can be evaluated, P_{AB}^0 is determined from eq 11. In most applications, P_{AB}^0 is considerably more tedious to calculate, so eq 11 provides a major simplification of the algebra. A related simplification is discussed in subsection D (and in Appendix A) below for the general situation of unequal refractive-index increments.

As emphasized previously, the results of light-scattering measurements of $\langle S^2\rangle_{app}$ depend on the diblock copolymer's refractive index increments, λ_A and λ_B. Equation 11, as applied to the radius of gyration, is not directly applicable to the experiments unless $\lambda_A = \lambda_B$. We consider this special case to outline certain features used also in providing similar simplifications of the general situation.

The ideal parts of $\langle S^2\rangle$ from eq 5 are given by

$$\hat{G}_I^0(N_A^0,N_B^0) = (N_A^0 l_A + N_B^0 l_B)^2/2 \tag{12a}$$

and

$$\hat{G}_I^{0\prime\prime}(N_A^0,N_B^0) = -d(N_A^0 l_A + N_B^0 l_B)^3/6 \tag{12b}$$

The first-order coefficients of the expansion in v_A^0 are

$$(2\pi)^2 v_A^0 \delta\hat{G}_A^0(N_A^0,N_B^0) = -u_A^0(N_A^0 l_A + N_B^0 l_B)^2\left(\frac{1}{\epsilon}+\frac{1}{2}+\frac{A}{2}\right) \tag{12c}$$

and

$$\begin{aligned}(2\pi)^2 v_A^0 \delta\hat{G}_A^{0\prime\prime}(N_A^0,N_B^0) = {} & d u_A^0\left\{\frac{1}{\epsilon}\left[\frac{2(N_A^0 l_A)^3}{3}+\right.\right.\\ & \left.2(N_A^0 l_A)^2 N_B^0 l_B + N_A^0 l_A (N_B^0 l_B)^2 + (N_B^0 l_B)^3/3\right] +\\ & \left[-\left(\frac{1}{72}+\frac{A}{3}\right)(N_A^0 l_A)^3 + \left(A-\frac{1}{12}\right)(N_A^0 l_A)^2 N_B^0 l_B +\right.\\ & \left.\left.\left(\frac{1}{2}+\frac{A}{2}\right)N_A^0 l_A (N_B^0 l_B)^2 + \left(\frac{1}{6}+\frac{A}{6}\right)(N_B^0 l_B)^3\right]\right\}\end{aligned} \tag{12d}$$

where $u_A^0 = v_A^0 L^\epsilon$, L is a phenomenological length scale[22] introduced to form a dimensionless interaction parameter, and

$$A = \ln\left(\frac{2\pi N_A{}^0 l_A}{L^2}\right) \tag{12e}$$

The radius of gyration of a homopolymer of length $N_A{}^0$ may be obtained from eq 5 by just setting $v_{AB}{}^0 = v_B{}^0 = 0$. Substituting only the first of the ideal diagrams and diagrams a–f from Figure 1 into that eq 5, we find

$$\langle S_A{}^2\rangle_H{}^0 = \frac{N_A{}^0}{6} l_A\left\{1 + u_A{}^0\left[\frac{2}{\epsilon} - \frac{13}{12} + A\right] + O(\epsilon)\right\} \tag{13}$$

in agreement with previous homopolymer calculations[2,5] where the subscript H designates that eq 13 applies to the A homopolymer. If we had taken $v_{AB}{}^0 = v_B{}^0 = v_A{}^0 = v^0$ and had defined $u^0 = v^0 L^\epsilon$, upon summing all diagrams, we would have obtained

$$\langle S_{A+B}{}^2\rangle_H{}^0 = \frac{(N_A{}^0 l_A + N_B{}^0 l_B)}{6}\left\{1 + u^0\left[\frac{2}{\epsilon} - \frac{13}{12} + C\right] + O(\epsilon)\right\} \tag{14}$$

with

$$C = \ln\left[2\pi(N_A{}^0 l_A + N_B{}^0 l_B)/L^2\right] \tag{15}$$

Equation 14 is more simply obtained from eq 13 by replacing $N_A{}^0 l_A$ with $N_A{}^0 l_A + N_B{}^0 l_B$ and A with C. By use of eq 12a–d in eq 5 to determine the coefficients of $v_A{}^0$ and $v_B{}^0$ in eq 10, eq 11 leads to

$$(2\pi)\frac{v^0}{2d}\left[\frac{\delta\hat{G}_{AB}{}^{0\prime\prime}(N_A{}^0,N_B{}^0)}{\hat{G}_I{}^{0\prime\prime}(N_A{}^0,N_B{}^0)} - \frac{\delta\hat{G}_{AB}{}^0(N_A{}^0,N_B{}^0)}{\hat{G}_I{}^0(N_A{}^0,N_B)}\right] = u^0\left[2(A-B)x_A{}^{0^3} + \left(-\frac{1}{4} - 3A + 3B\right)x_A{}^{0^2} + \frac{x_A{}^0}{4} + (C-B)\right] \tag{16}$$

with

$$B = \ln\left(2\pi N_B{}^0 l_B/L^2\right) \tag{17a}$$

and

$$x_A{}^0 = N_A{}^0 l_A/(N_A{}^0 l_A + N_B{}^0 l_B) \tag{17b}$$

Notice that eq 16 has been derived without evaluating any of the AB diagrams. Subsection D describes similar simplifications for the general $\lambda_A \neq \lambda_B$ case. Equation 16 holds even when $v^0 \neq v_{AB}{}^0 \neq v_B{}^0$. Having determined the coefficient of $v_{AB}{}^0$ for $\langle S^2\rangle^0$, we can use eq 12a–d and 16 to determine $\langle S^2\rangle$ in the general, three interaction parameter case. The new result is

$$\langle S^2\rangle^0 = \frac{(N_A{}^0 l_A + N_B{}^0 l_B)}{6}\left\{1 + u_A{}^0\left[\frac{(6x_A{}^{0^2} - 4x_A{}^{0^3})}{\epsilon} + \left(\frac{29}{12}x_A{}^{0^3} - \frac{7}{2}x_A{}^{0^2}\right) + (3x_A{}^{0^2} - 2x_A{}^{0^3})A\right] + u_{AB}{}^0\left[2(A - B)x_A{}^{0^3} + \left(-\frac{1}{4} - 3A + 3B\right)x_A{}^{0^2} + x_A{}^{0^2} + x_A{}^0 + (C-B)\right] + u_B{}^0\left[\frac{4x_A{}^{0^3} - 6x_A{}^{0^2} + 2}{\epsilon} + \left(-\frac{29}{12}x_A{}^{0^3} - \frac{15}{4}x_A{}^{0^2} - \frac{x_A{}^0}{4} - \frac{13}{12}\right) + (2x_A{}^{0^3} - 3x_A{}^{0^2} + 1)B\right]\right\} \tag{18}$$

C. The Renormalized $\langle S^2\rangle$. Equation 18 contains singularities in ϵ which arise because cutoffs[23] have been neglected in eq 1.[2] These unphysical singularities must be removed to make the equations application in the $d = 4$, $\epsilon = 0$ limit. One way to do this is to replace the bare quantities, $\langle S^2\rangle^0$, $u_A{}^0$, $u_{AB}{}^0$, $N_A{}^0$, etc., by their renormalized counterparts as defined through

$$\langle S^2\rangle = Z_{S^2}{}^{-1}\langle S^2\rangle^0 \tag{19a}$$

$$u_A = Z_{u_A}{}^{-1} u_A{}^0 \tag{19b}$$

$$u_{AB} = Z_{u_{AB}}{}^{-1} u_{AB}{}^0 \tag{19c}$$

$$u_B = Z_{u_B}{}^{-1} u_B{}^0 \tag{19d}$$

$$N_A = Z_{N_A} N_A{}^0 \tag{19e}$$

and

$$N_B = Z_{N_B} N_B{}^0 \tag{19f}$$

The renormalization constants in eq 19a–f are chosen to cancel the singularities in $\langle S^2\rangle^0$.

Instead of proceeding in this fashion, we appeal to previous discussions of the diblock polymer radius of gyration which consider $\langle S^2\rangle$ relative to homopolymer quantities. Following ref 13, we define $\delta_1{}^0$ by

$$\langle S^2\rangle^0 = x_A{}^0\langle S_A{}^2\rangle_H{}^0 + (1 - x_A{}^0)\langle S_B{}^2\rangle_H{}^0 + 2x_A{}^0(1 - x_A{}^0)[\langle S_A{}^2\rangle_H{}^0 + \langle S_B{}^2\rangle_B{}^0]\delta_1{}^0 \tag{20}$$

where $\langle S_A{}^2\rangle_H{}^0$ and $\langle S_B{}^2\rangle_H{}^0$ are the bare homopolymer radii of gyration of A and B chains having the same length and excluded-volume parameters as the precursors of the A and B blocks. The quantity $\delta_1{}^0$ provides a measure of the influence of the interblock interactions, and $\delta_1{}^0$ equals unity when the solution is ideal with respect to all three interaction parameters ($u_A{}^0 = u_B{}^0 = u_{AB}{}^0 = 0$). Equation 20 must contain the same singularities as eq 18.

If we substitute eq 18 for the left-hand side of eq 20 and use eq 13 and its analogue for $\langle S_B{}^2\rangle_H{}^0$, we obtain

$$\delta_1{}^0 = 1 - \frac{x_A{}^0}{8}u_A{}^0 - \frac{x_B{}^0}{8}u_B{}^0 + u_{AB}{}^0\left[\frac{1}{8} + \frac{(2x_A{}^0 - 3)}{2x_B{}^0}x_A{}^0 \ln x_A{}^0 + \frac{(2x_B{}^0 - 3)}{2x_A{}^0}x_B{}^0 \ln x_B{}^0\right] \tag{21}$$

having defined $x_B{}^0 = 1 - x_A{}^0$. This contains no singularities, and to an accuracy of order ϵ, each term in eq 21 may be replaced with its renormalized counterpart. (A renormalized δ_1 is defined through the equation obtained from eq 20 by removing all superscript zeros.) Thus, the renormalized reduced ratio δ_1 becomes

$$\delta_1 = 1 - \frac{x_A}{8}u_A - \frac{x_B}{8}u_B + u_{AB}\left[\frac{1}{8} + \frac{(2x_A - 3)}{2x_B}x_A \ln x_A + \left(\frac{2x_B - 3}{2x_A}\right)x_B \ln x_B\right] \tag{22}$$

The well-known[2,5] renormalized expressions for the homopolymer radii of gyration $\langle S_A{}^2\rangle_H$ and $\langle S_B{}^2\rangle_H$ are

$$\langle S_i^2\rangle_H = \frac{N_i l_i}{6}\left[1 + u_i\left(-\frac{13}{12} + \ln\frac{2\pi N_i}{L}\right)\right] \qquad i = A, B \tag{23}$$

The renormalized versions of eq 20–23 provide the renormalized radius of gyration of the diblock chain.

D. Unequal Refractive Index Increments and Simplification of AB Diagrams. The calculations with

unequal refractive index increments are somewhat more complicated than the simple derivation just outlined for $\lambda_A = \lambda_B$. While the configuration of the diblock chain depends only on the solvent characteristics, the apparent radius of gyration $\langle S^2\rangle_{app}$ measured in light-scattering experiments is sensitive to λ_A and λ_B. For instance, diagrams like a–f in Figure 1 are weighted by a factor of λ_A^2, whereas diagrams g–i contribute proportional to $\lambda_A\lambda_B$ to the overall light-scattering intensity. Because of this, a relation analogous to eq 10 does not hold for $\langle S^2\rangle_{app}$. Fortunately, a number of symmetry and topological relations exist between the diagrams which again simplify their calculation. Appendix A describes these relations in detail. Here, we quote only the essential results.

When $\lambda_A \neq \lambda_B$, the generalization[12] of eq 20 is

$$\langle S^2\rangle_{app}{}^0 = \mu_A{}^0\langle S_A{}^2\rangle_H{}^0 + \mu_B{}^0\langle S_B{}^2\rangle_H{}^0 + 2\mu_A{}^0\mu_B{}^0[\langle S_A{}^2\rangle_H{}^0 + \langle S_B{}^2\rangle_H{}^0]\delta_2{}^0 \quad (24)$$

where the $\mu_i{}^0$ are defined by

$$\mu_A{}^0 = \lambda_A x_A{}^0/[\lambda_A x_A{}^0 + \lambda_B x_B{}^0] \quad (25a)$$

and

$$\mu_B{}^0 = 1 - \mu_A{}^0 \quad (25b)$$

The bare apparent radius of gyration is obtained to first order in ϵ and the u^0's by summing all of the λ-weighted diagrams. Employing the same line of reasoning that leads to eq 21, we obtain

$$\delta_2 = 1 - \frac{x_A}{8}u_A - \frac{x_B u_B}{8} + u_{AB}\Big\{[-(7/2)\mu_A{}^2 x_A x_B + 3\mu_A{}^2 - 4\mu_A x_A + \mu_A x_A{}^2 + x_A{}^3(2 - 3\mu_A) + (5/4)x_A{}^2 - x_A{}^4/4]/(2x_A x_B\mu_A\mu_B) - [(\mu_A x_A{}^2 - (5/2)\mu_A x_A + 3\mu_A - (3/2)x_A]\frac{x_A \ln x_A}{\mu_A x_B{}^2} - [\mu_B x_B{}^2 - (5/2)\mu_B x_B + 3\mu_B - (3/2)x_B]\frac{x_B \ln x_B}{\mu_B x_A{}^2}\Big\} \quad (26)$$

The apparent radius of gyration, as measured in light-scattering experiments, is again calculated by replacing the bare quantities in eq 24 with their renormalized counterparts. Equations 23 and 26 provide the latter.

E. Alternative Representations of the Radius of Gyration. The definition of the apparent radius of gyration, eq 24, in terms of homopolymer radii of gyration leads to a complicated functional dependence of δ_2 on μ_A and μ_B. A somewhat more compact representation emerges upon defining δ_3 by

$$\langle S^2\rangle_{app} = \mu_A\langle S_A{}^2\rangle + \mu_B\langle S_B{}^2\rangle + 2\mu_A\mu_B(\langle S_A{}^2\rangle + \langle S_B{}^2\rangle)\delta_3 \quad (27)$$

where $\langle S_A{}^2\rangle$ and $\langle S_B{}^2\rangle$ are the radii of gyration of the A and B blocks in the block copolymer. Note that

$$\langle S_i{}^2\rangle \neq \langle S_i{}^2\rangle_H \qquad i = A, B$$

except when $u_A = u_B = u_{AB} = 0$. By taking the $\mu_A \to 0$ limit of the renormalized counterpart of eq 24 and by using eq 26, we may evaluate the convenient dimensionless ratios of Tanaka et al.[12]

$$\gamma_i = \frac{\langle S_i{}^2\rangle}{\langle S_i{}^2\rangle_H} = 1 + \frac{u_{AB}}{x_i}\left[\frac{(1 - x_i)}{4x_i}(12 - 6x_i - x_i{}^2) + 3\frac{(1 - x_i)^2}{x_i{}^2}\ln(1 - x_i)\right] \qquad i = A, B \quad (28)$$

Comparing eq 27 and the renormalized eq 24 and using eq 28 enable us to deduce the renormalized expression

$$\delta_3 = 1 - \frac{x_A}{8}u_A - \frac{x_B}{8}u_B - u_{AB}\Big\{(x_A{}^2 + x_A/2 + 3)\frac{x_A}{x_B{}^2}\ln x_A + (x_B{}^2 + x_B/2 + 3)\frac{x_B}{x_A{}^2}\ln x_B + [9/2 - (37/4)x_A + (35/4)x_A{}^2 + x_A{}^3 - x_A{}^4/2]/(x_A x_B)\Big\} \quad (29)$$

Notice that δ_3 is independent of μ_A and μ_B. Equation 27 may also be written as

$$\langle S^2\rangle_{app} = \mu_A\langle S_A{}^2\rangle + \mu_B\langle S_B{}^2\rangle + \mu_A\mu_B\langle(\mathbf{z}_A - \mathbf{z}_B)^2\rangle \quad (30)$$

where $\mathbf{z}_A$ and $\mathbf{z}_B$ denote the centers of mass of the A and B blocks. The comparison of eq 27 and 28 implies that δ_3 has the interpretation[16]

$$\delta_3 = \langle(\mathbf{z}_A - \mathbf{z}_B)^2\rangle[2(\langle S_A{}^2\rangle + \langle S_B{}^2\rangle)]^{-1} \quad (31)$$

Hence, δ_3 provides a measure of the center-of-mass separation of the two blocks, while δ_1 or, more generally, δ_2 represents the extent to which the blocks deviate from statistical independence. In the ideal $u_A, u_B, u_{AB} \to 0$ limit, δ_1, δ_2, and δ_3 all approach unity.

F. The Scaling Limit. When $\lambda_A = \lambda_B$ and in the good-solvent scaling limit $u_A = u_B = u_{AB} = u^*$, eq 20 can be solved for δ_1 exactly.[13] Use of the scaling limit

$$\langle S_i{}^2\rangle_H \sim N_i{}^{2\nu} \qquad i = A, B \quad (32)$$

in eq 20 yields

$$\delta_1(u^*) = \frac{\{1 - [x_A{}^{2\nu+1} + x_B{}^{2\nu+1}]\}}{2x_A x_B[x_A{}^{2\nu} + x_B{}^{2\nu}]} \quad (33)$$

Equation 22 for δ_1 is only correct to first order in the interaction potentials. We can extend the range of usefulness of eq 22 by first making it consistent with the scaling limit in (33). This procedure motivates the reexponentiation[13] in (22) to

$$\delta_1 = (u_{AB} - x_A u_A - x_B u_B)/8 + [1 - (x_A{}^{u_{AB}+2} + x_B{}^{u_{AB}+2})][2x_A x_B(x_A{}^{u_{AB}+1} + x_B{}^{u_{AB}+1})]^{-1} \quad (34)$$

The exact strong-coupling, scaling behavior of $\langle S^2\rangle_{app}$ as a function of x_A and x_B is not known for $\lambda_A \neq \lambda_B$. Hence, the arguments leading to eq 37 cannot be used to derive a similar expression for δ_2. If we express $\langle S^2\rangle_{app}$ in terms of $\langle S_i^2\rangle_H$ (i = A, B) and δ_3, however, and assume that δ_3 does not depend on λ_A and λ_B, we may rewrite (29) in the reexponentiated form

$$\delta_3(u^*) = \frac{\{1 - [\gamma_A x_A{}^{2\nu+1} + \gamma_B x_B{}^{2\nu+1}]\}}{2x_A x_B(\gamma_A x_A{}^{2\nu} + \gamma_B x_B{}^{2\nu})} \quad (35)$$

in the good-solvent limit, where the γ_i (i = A, B) are defined in the left side of (31). An expression consistent with both eq 29 and 35 is

$$\delta_3 = (u_{AB} - x_A u_A - x_B u_B)/8 + [1 - (\gamma_A x_A{}^{u_{AB}+2} + \gamma_B x_B{}^{u_{AB}+2})][2x_A x_B(\gamma_A x_A{}^{u_{AB}+1} + \gamma_B x_B{}^{u_{AB}+1})]^{-1} \quad (36)$$

Equation 33 is the homopolymer limit ($u_A = u_B = u_{AB} \to u^*$) of (36). We are unaware of other simple scaling lawa that would place additional constraints on the analytic structure of δ_1 and δ_3. Nevertheless, as discussed below, our theoretical expressions agree well with available Monte Carlo simulations and experimental data. Equations 28 and 36, used in conjunction with eq 27, provide the ap-

Table I
Summary of Equations for the Apparent Radius of Gyration[a]

$$\gamma_i = 1 + \left[\frac{(4\bar{z}_{AB}/3)f(\bar{z}_A,\bar{z}_B)}{1 + (16/3)g(\bar{u}_A,\bar{u}_B)\bar{z}_{AB}f(\bar{z}_A,\bar{z}_B)}\right]\frac{1}{x_i}\left[\frac{(1-x_i)}{4x_i}(12 - 6x_i - x_i^2) + 3\frac{(1-x_i)^2}{x_i^2}\ln(1-x_i)\right] \qquad i = A, B$$

$$\delta_2 = 1 - \frac{(\bar{z}_A/6)x_A}{1 + (32/3)\bar{z}_A} - \frac{(\bar{z}_B/6)x_B}{1 + (32/3)\bar{z}_B} + \frac{(4\bar{z}_{AB}/3)f(\bar{z}_A,\bar{z}_B)}{1 + (16/3)g(\bar{u}_A,\bar{u}_B)\bar{z}_{AB}f(\bar{z}_A,\bar{z}_B)}\Big\{[-(7/2)\mu_A^2x_Ax_B + 3\mu_A^3 - 4\mu_Ax_A + \mu_Ax_A^2 + x_A^3(2 - 3\mu_A) +$$
$$(5/4)x_A^3 - x_A^4/4](2x_Ax_B\mu_A\mu_B)^{-1} - [\mu_Ax_A^2 - (5/2)\mu_Ax_A + 3\mu_A - (3/2)x_A]\frac{x_A\ln x_A}{\mu_Ax_B^2} - [\mu_Bx_B^2 - (5/2)\mu_Bx_B + 3\mu_B - (3/2)x_B)]\frac{x_B\ln x_B}{\mu_Bx_A^2}\Big\}$$

$$\delta_1 = \frac{(\bar{z}_{AB}/6)f(\bar{z}_A,\bar{z}_B)}{1 + (16/3)g(\bar{u}_A,\bar{u}_B)\bar{z}_{AB}f(\bar{z}_A,\bar{z}_B)} - \frac{x_A\bar{z}_A/6}{1 + (32/3)\bar{z}_A} - \frac{x_B\bar{z}_B/6}{1 + (32/3)\bar{z}_B} + \{1 - [x_A^{2+[(4\bar{z}_{AB}/3)f(\bar{z}_A,\bar{z}_B)]/[1+(16/3)g(\bar{u}_A,\bar{u}_B)\bar{z}_{AB}f(\bar{z}_A,\bar{z}_B)]} +$$
$$x_B^{2+[(4\bar{z}_{AB}/3)f(\bar{z}_A,\bar{z}_B)]/[1+(16/3)g(\bar{u}_A,\bar{u}_B)\bar{z}_{AB}f(\bar{z}_A,\bar{z}_B)]}]\}\{2x_Ax_B[x_A^{1+[(4\bar{z}_{AB}/3)f(\bar{z}_A,\bar{z}_B)]/[1+(16/3)g(\bar{u}_A,\bar{u}_B)\bar{z}_{AB}f(\bar{z}_A,\bar{z}_B)]} + x_B^{1+[(4\bar{z}_{AB}/3)f(\bar{z}_A,\bar{z}_B)]/[1+(16/3)g(\bar{u}_A,\bar{u}_B)\bar{z}_{AB}f(\bar{z}_A,\bar{z}_B)]}]\}^{-1}$$

$$\delta_3 = \frac{(\bar{z}_{AB}/6)f(\bar{z}_A,\bar{z}_B)}{1 + (16/3)g(\bar{u}_A,\bar{u}_B)\bar{z}_{AB}} - \frac{x_A\bar{z}_A/6}{1 + (32/3)\bar{z}_A} - \frac{x_B\bar{z}_B/6}{1 + (32/3)\bar{z}_B} + \{1 - [\gamma_Ax_A^{2+(4\bar{z}_{AB}/3)/[1+(16/3)g(\bar{u}_A,\bar{u}_B)\bar{z}_{AB}f(\bar{z}_A,\bar{z}_B)]} +$$
$$\gamma_Bx_B^{2+[(4\bar{z}_{AB}/3)f(\bar{z}_A,\bar{z}_B)]/[1+(16/3)g(\bar{u}_A,\bar{u}_B)\bar{z}_{AB}f(\bar{z}_A,\bar{z}_B)]}]\}\{2x_Ax_B[\gamma_Ax_A^{1+[(4\bar{z}_{AB}/3)f(\bar{z}_A,\bar{z}_B)]/[1+(16/3)g(\bar{u}_A,\bar{u}_B)\bar{z}_{AB}f(\bar{z}_A,\bar{z}_B)]} +$$
$$\gamma_Bx_B^{1+[(4\bar{z}_{AB}/3)f(\bar{z}_A,\bar{z}_B)]/[1+(16/3)g(\bar{u}_A,\bar{u}_B)\bar{z}_{AB}f(\bar{z}_A,\bar{z}_B)]}]\}^{-1}$$

[a] See eq 20, 24, 27, and 28 for the defintions of δ_1, δ_2, δ_3, and γ_i.

parent radius of gyration and are the main result of this paper.

G. Crossover Scaling Variables. The radius of gyration, like all long-wavelength polymer properties, obeys a renormalization group equation and certain formal scaling relations.[2,13] These define three crossover scaling variables, ζ_A, ζ_B, and ζ_{AB}, in terms of the three interaction parameters in the problem. Inversion of these relations so that u_A, u_B, and u_{AB} can be written as functions of ζ_A, ζ_B, and ζ_{AB} and subsequent substitution into the formulas for the radius of gyration ensure that our results are consistent with the renormalization group equation.

The exact order ϵ crossover analysis has been discussed previously, and we refer the interested reader to ref 13 and 24 for the details. In order to make as much contact as possible between traditional TP theories and the RG predictions, these studies transform the ζ's into expressions with empirical z-parameters. In $d = 3$, this amounts to the use of the substitutions (for $\epsilon = 1$) in renormalized quantities of

$$u_i = (1/8)\frac{(32/3)\bar{z}_i}{1 + (32/3)\bar{z}_i}, \qquad i = A, B \tag{37a}$$

and (correcting an error in eq C7 of ref 24)

$$u_{AB} = \frac{(4\bar{z}_{AB}/3)f(\bar{z}_A,\bar{z}_B)}{1 + (16/3)g(\bar{u}_A,\bar{u}_B)\bar{z}_{AB}f(\bar{z}_A,\bar{z}_B)} \tag{37b}$$

where (for $\epsilon = 1$)

$$\bar{u}_i = 8u_i \qquad i = A, B \tag{37c}$$

$$g(\bar{u}_A,\bar{u}_B) = \int_0^1 d\tau\,(1 - \tau\bar{u}_A)^{-1/4}(1 - \tau\bar{u}_B)^{-1/4} \tag{37d}$$

and

$$f(\bar{z}_A,\bar{z}_B) = [(1 + 32\bar{z}_A/3)(1 + 32\bar{z}_B/3)]^{-1/4} \tag{37e}$$

For convenience in comparisons with experiment eq 37a–e are substituted into (26), (28), (34), and (36) to produce the final results summarized in Table I.

III. Comparison to Monte Carlo Simulations

As mentioned in the introduction, accurate experimental determinations of the radius of gyration do not exist. It is our goal here to make some qualitative comparisons to Monte Carlo simulations[12] with the hope that our predictions for δ_1, δ_3, etc. can be used in future experimental efforts to determine $\langle S^2\rangle$ for block copolymers.

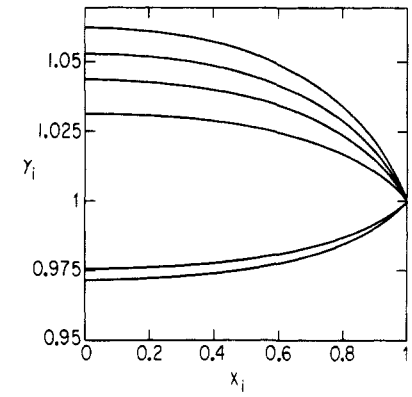

Figure 2. Dependence of the block expansion factor γ_i (i = A, B) on composition for several solvent conditions. Starting from the top we have $\bar{z}_A = \bar{z}_B = 0$, $\bar{z}_{AB} = \infty$; $\bar{z}_A = \bar{z}_B = 0.1$, $\bar{z}_{AB} = \infty$; $\bar{z}_A = \bar{z}_B = 0.5$, $\bar{z}_{AB} = \infty$; $\bar{z}_A = \bar{z}_B = \bar{z}_{AB} = \infty$; $\bar{z}_A = \bar{z}_B = 1.0$, $\bar{z}_{AB} = -0.2$; and $\bar{z}_A = \bar{z}_B = 0.1$, $\bar{z}_{AB} = -0.2$.

One interesting observation of Tanaka et al.[12a] concerns the block expansion factors γ_A and γ_B. These authors have performed Monte Carlo simulations for diblock chains on a cubic lattice with $x_A = x_B = {}^1/_2$ and $\bar{z}_A = \bar{z}_B = 0$, while rejecting configurations for which A and B segments occupy the same site. The simulations show that $\gamma_A = \gamma_B = 1.02$. This case corresponds to our theory with $u_A = u_B = 0$ and $u_{AB} \leq 0.25$ (see eq 37b). For $x_A = {}^1/_2$, we compute

$$\gamma_A \leq 1.05$$

from eq 28, in fair agreement with the Monte Carlo work. Figure 2 plots the variation of γ_i versus x_i for several values of u_{AB}. Even at the maximum fixed-point $\epsilon/4$ value of u_{AB}, (or ${}^1/_4$ for $d = 3$), the heterocontacts do little to perturb the sizes of the individual blocks.[12,13] In poorer solvents (i.e., $u_{AB} < \epsilon/4$), the AB interactions should affect the sizes of the A and B blocks relative to the homopolymer even less. Figure 2 also presents two plots for the case $\bar{z}_{AB} < 0$ (i.e., attractive AB interactions). This type of interaction tends to pull the blocks together, while making them more compact. The γ_i's for attractive AB heterocontacts approach unity as the solvent quality improves for the homopolymers, the role of the AB interactions becoming less important as the homopolymers swell.

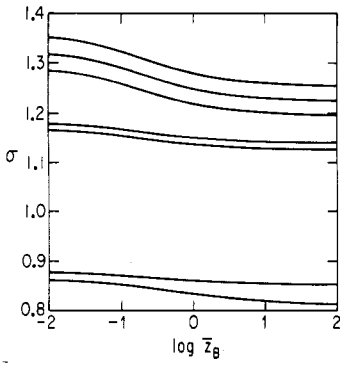

Figure 3. Quantity σ from eq 38 versus B-solvent quality for several values of $\bar{z}_A$ and $\bar{z}_{AB}$. From the top we have $\bar{z}_A = 0$, $\bar{z}_{AB} = \infty$; $\bar{z}_A = 0.1$, $\bar{z}_{AB} = \infty$; $\bar{z}_A = 0.5$, $\bar{z}_{AB} = \infty$; $\bar{z}_A = 0.1$, $\bar{z}_{AB} = 1.0$; $\bar{z}_A = 0.5$, $\bar{z}_{AB} = 1.0$; $\bar{z}_A = 0$, $\bar{z}_{AB} = -0.1$; and $\bar{z}_A = 0.5$, $\bar{z}_{AB} = -0.1$.

Reference 12a also discusses the limiting case $\bar{z}_{AB} = \bar{z}_A = \bar{z}_B$ in terms of the ratio

$$\sigma = \frac{\langle |\mathbf{z}_A - \mathbf{z}_B|^2 \rangle}{2(\langle S_A^2 \rangle_H + \langle S_B^2 \rangle_H)} = \delta_3 \left[\frac{\gamma_A \langle S_A^2 \rangle_H + \gamma_B \langle S_B^2 \rangle_H}{\langle S_A^2 \rangle_H + \langle S_B^2 \rangle_H} \right] \quad (38)$$

the second equality following from eq 28 and 31. Our calculations predict $\sigma = 1.36$ for $x_A = {}^1/_2$ in the limit $\bar{z}_A = \bar{z}_B = 0$ and $\bar{z}_{AB} \to \infty$, in good agreement with the 1.43 quoted in ref 12a,d. In the homopolymer-equivalent case, where all three interaction parameters are equal, the presence of A- and B-intrablock repulsions cause the blocks to swell, reducing the likelihood of A–B heterocontacts. At the $\bar{z}_A$, $\bar{z}_B$, and $\bar{z}_{AB} \to \infty$ fixed point, we compute $\sigma = 1.15$, which compares reasonably well to estimates, deduced from simulations of self-avoiding chains on a tetrahedral lattice,[25] in the range[12a] 1.16–1.25. The overall radius of gyration expansion factor α_{AB}^2 is the ratio of $\langle S^2 \rangle$ for the diblock chain to the ideal one for which $\langle S^2 \rangle_I = (N_A l_A + N_B l_B)/6$. For the common Θ-solvent case where $\bar{z}_A = \bar{z}_B = 0$ but $\bar{z}_{AB} \to \infty$, we evaluate $\delta_1 = 1.41$ from eq 34 or Table I. Using this result in the renormalized version of eq 20 gives

$$\alpha_{AB}^2 = 1.23$$

compared to the earlier[13] estimate of 1.19 and in excellent agreement with the simulations' value of 1.22.[12a] (Power law exponents of N_A and N_B are unaffected in the common Θ limit, so second-order corrections are not expected to be required there.)

Douglas and Freed[13] have previously compared a combination of TP model calculations[17] and the RG theory for a diblock chain to the Monte Carlo simulations. In every case, our results agree with the earlier ones[13] to within 4%, providing a consistency check on our calculations. That the two sets of results differ at all can be attributed to our use of explicit RG calculations (in a reexponentiated version), as opposed to the use of the $d = 3$ TP model calculations and RG theory in ref 13. The present paper is more general and describes the entire range of diblock copolymer compositions (i.e., $x_A \neq x_B$), temperature, and solvent conditions.

Finally, we compare the predictions of the equations in Table I to simulations[12e] which assume $x_A = {}^1/_2$, $\bar{z}_{AB} = \infty$, and one or both of $\bar{z}_A$ and $\bar{z}_B \neq 0$. Figure 3 presents several plots of σ versus $\bar{z}_B$ for specific choices of $\bar{z}_A$ and $\bar{z}_{AB}$. As the A and B blocks swell, the importance of AB interactions lessens and σ decreases. Such behavior is indicated in the top three plots in Figure 3. Each of these takes $\bar{z}_{AB} = \infty$ but $\bar{z}_A$ increases from 0 in the top curve to 0.1 and 0.5 in the second and third plots. The same trend is observed in the simulations. Reference 12e plots σ versus a B interaction variable for the specific case $\bar{z}_A = 0$ and $\bar{z}_{AB} = \infty$. The curve generated for this Monte Carlo data looks very much like the equivalent plot of Figure 3.

The fourth and fifth curves show the effects of decreasing $\bar{z}_{AB}$ to 1.0 for $\bar{z}_A = 0.1$ and 0.5. The differences between the first group of three plots and the latter two illustrate the slow crossover behavior of the $\bar{z}_{AB}$ variable. In contrast, values of $\bar{z}_A$ and $\bar{z}_B$ near 1.0, by virtue of the large prefactor in the denominator of eq 37a, imply that u_A and u_B have nearly approached their good-solvent fixed-point limits of ${}^1/_8$ ($d = 3$). However, u_{AB} approaches its large $\bar{z}_{AB}$ asymptote more slowly because $(16/3)g(\bar{u}_A,\bar{u}_B) \leq {}^{32}/_3$ for all $\bar{z}_A$ and $\bar{z}_B \geq 0$. A different behavior dominates as $\bar{z}_A$ and/or $\bar{z}_B \to \infty$. In this limit, u_{AB} vanishes as $z_i^{-1/4}$ (i = A, B) and we find that $\sigma = 1$.

When $\bar{z}_{AB}$ is negative, the attractions between the blocks tends to pull them together. The theory predicts that this behavior is most pronounced when $\bar{z}_A$ and $\bar{z}_B$ are small and the denominator of eq 37b is, therefore, small, resulting in a large, negative value for u_{AB}. The bottom two plots of Figure 3 illustrate this phenomenon. Lacking any experimental or simulation data to compare our results to, we are unable to comment, at this time, whether these trends accurately reflect the behavior of diblock chains in the presence of weakly attractive AB interactions.

IV. Discussion

The equations that we have derived for the γ_i's and the δ parameters, δ_1, δ_2, and δ_3, describing the radius of gyration, agree semiquantitatively with all of the Monte Carlo results discussed in the previous section. Therefore, we expect similar accuracy upon extending our results to more general situations ($x_A \neq {}^1/_2$, variable $\bar{z}$'s) including ones of relevance to experimental situations. For polystyrene–poly(methyl methacrylate) (PS–PMMA) diblocks in methyl ethyl ketone (MEK),[12c] σ appears to vary between 1.10 and 1.30, depending on the relative sizes of the A and B blocks. MEK is a good solvent for both PS and PMMA, which suggests that σ should be significantly less than the 1.43 of the simulations. That the theory predicts this is encouraging. Precise, experimental data for σ in monodisperse systems are presently unavailable, so we cannot comment more fully on the quantitative agreement with experiment. There may be some quantitative discrepancies by virtue of our use of a first-order perturbation analysis, but the focus on reduced variables makes such a treatment more accurate than that applied to quantities such as $\langle S_A^2 \rangle$ whose power law exponents are significantly altered by second-order corrections.

A likely experimental situation consists of $\bar{z}_A \gg 1$, a good solvent for the A block, $\bar{z}_B \ll 1$, near the B-block Θ state, and $\bar{z}_{AB}$ variable. Except when the AB interactions are attractive, the computed block expansion factors do not differ from unity by more than several percent. Measurements of σ provide a more sensitive gauge of the interblock interactions. Figure 4 presents plots of σ versus $\bar{z}_{AB}$ for $\bar{z}_A \to 10$, a pair of values of $\bar{u}_B$, and several possible compositions. At fixed composition, σ increases significantly with the strength of the AB interblock interactions and decreases as the B intrablock interactions become stronger. Near the B-block Θ region, we can expand the integrand of eq 37d in a power series in $\bar{u}_B$. This results in

$$g(\bar{u}_A,\bar{u}_B) = \frac{4}{3\bar{u}_A}[1 - (1 - \bar{u}_A)^{3/4}] + \frac{4\bar{u}_B}{21\bar{u}_A^2}[1 - (1 + (3/4)\bar{u}_A)(1 - \bar{u}_A)^{3/4}] + O(\bar{u}_B^2) \quad (39)$$

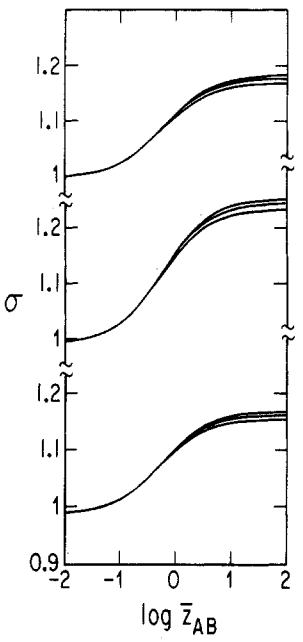

Figure 4. σ versus $\bar{z}_{AB}$ near the B-block Θ point for $\bar{z}_A = 10$. Upper three curves, $x_A = 0.2$, $x_B = 0.8$; middle three curves, $x_A = x_B = 0.5$; bottom three curves, $x_A = 0.8$, $x_B = 0.2$. Within each set, the top curve has $\bar{u}_B = 0$, the middle one $\bar{u}_B = 0.2$, and the bottom one $\bar{u}_B = 0.4$. (Note that eq 37a–c relate $\bar{u}_B$ to $\bar{z}_B$.)

which approximates the exact $g(\bar{u}_A,\bar{u}_B)$ to within half a percent for $\bar{u}_B \leq 0.4$, providing a simpler alternative to the full integral which must otherwise be evaluated numerically.

Our computations display a series of trends that may be visualized rather simply. When the interblock interactions are large, an increase in intrablock excluded volume tends to swell the individual blocks, thereby minimizing the interblock contacts and, therefore, the influence of the interblock interactions on individual block dimensions. These trends correspond directly to those found for the configuration of a polymer interacting with a surface, where the polymer–surface interactions play the role of the interblock excluded volume.[27]

The arguments that we present to deduce expressions for δ_1, δ_2, and δ_3 may be generalized to mixtures of homopolymers or more complicated block copolymers (e.g., ABA triblocks[13]). It may also be possible to develop an algebra of the three interaction parameter system to a higher order than ϵ^1 in perturbation theory. Without using such techniques, it appears enormously complicated to evaluate the complex diagrams that occur at order ϵ^2 and higher in such systems.

Acknowledgment. This research is supported, in part, by NSF DMR86-14358 (condensed matter theory program). W.E.M. thanks Professor David W. Oxtoby for financial support (NSF CHE-8520520).

Appendix A. Relationships between Diagrams

We introduce a notation which helps exhibit the useful relationships between the diagrams shown in Figure 1. Consider first the middle set whose sum, $\delta G_A{}^0(\mathbf{c}_{21};N_A{}^0,N_B{}^0)$, is the prefactor of $v_A{}^0$. Let the symbol A_γ specify each of these, where γ runs from a to j. Similarly, we use the notation

$$AB_\gamma \qquad \gamma = k, ..., t$$

to denote the diagrams contributing to $\delta G_{AB}{}^0(\mathbf{c}_{21};N_A{}^0,N_B{}^0)$. A third set—B diagrams—exists which forms the prefactor of $v_B{}^0$ but which is not listed in Figure 1 because it is obtained from the A set by interchanging $N_A{}^0 l_A$ and $N_B{}^0 l_B$. Using the same subscripts to designate members of the A and B sets, we have the simplest symmetry relation

$$B_\gamma(\mathbf{c}_{21};N_A{}^0,N_B{}^0) = A_\gamma(\mathbf{c}_{21};N_B{}^0,N_A{}^0) \qquad \gamma = a, b, ..., j \tag{A.1}$$

The B_γ's can also be viewed as reflections of the A_γ's through a plane perpendicular to the chain and passing through the center bar. During the remainder of the theoretical development, we simplify the notation by not explicitly indicating the dependence of the diagrams on $\mathbf{c}_{21}$, $N_A{}^0 l_A$, and $N_B{}^0 l_B$.

A number of obvious reflection symmetries also exist between members of the AB group of diagrams. These are

$$AB_k \leftrightarrow AB_r \tag{A.2a}$$

$$AB_l \leftrightarrow AB_s \tag{A.2b}$$

$$AB_m \leftrightarrow AB_t \tag{A.2c}$$

and

$$AB_o \leftrightarrow AB_p \tag{A.2d}$$

The diagrams on the right-hand side of these equations are trivially obtained from those on the left-hand side by exchanging $N_A{}^0 l_A$ and $N_B{}^0 l_B$ as in eq A.1. These relationships reduce to six the number of independent diagrams whose evaluation is required to characterize the AB set.

Now consider the set of (homopolymer) diagrams obtained by removing the center bars from the first six A_γ's. We denote these by C_γ, where $\gamma = a, ..., f$. Each of these is a function of $N_A{}^0 l_A + N_B{}^0 l_B$ but not of $N_A{}^0 l_A$ and $N_B{}^0 l_B$ separately. It also follows from the discussion surrounding eq 7 and from the normalization of $G_I{}^0(\mathbf{c}_\beta-\mathbf{c}_\alpha;\tau_\beta-\tau_\alpha)$ that the first six A_γ's are functions of $N_A{}^0 l_A$ but not of $N_B{}^0 l_B$. The integration over $\mathbf{c}_B(N_B{}^0)$ removes the B half from these, leaving a C diagram with $N_A{}^0 l_A + N_B{}^0 l_B$ replaced by $N_A{}^0 l_A$. Hence, we obtain the C_γ's from the A_γ's (with $\gamma = a, ..., f$) by replacing $N_A{}^0 l_A$ in the latter with $N_A{}^0 l_A + N_B{}^0 l_B$.

Finally, we present equations relating AB diagrams to the simpler A, B, and C ones. Recall that the integrations over a particular diagram's contour points (located at the ×'s and the ends of the dotted semicircle) range over all topologically consistent values. For example, the right-hand × of A_a varies from 0 to $N_A{}^0$ but cannot cross the center bar since A_g already contains such contributions to $\delta G_A{}^0(\mathbf{c}_{21};N_A{}^0 l_A,N_B{}^0)$. However, except for the location of the center bar, the diagrams A_a, A_g, A_j, AB_t, and B_e are identical. Their sum must, therefore, equal C_a, which corresponds to any one of these diagrams with the center bare removed. The same logic applies to other sets of topologically similar diagrams, and this analysis provides the useful relationships

$$C_a = A_a + A_g + A_j + AB_t + B_e \tag{A.3a}$$

$$C_b = A_b + A_n + AB_o + AB_s + B_d \tag{A.3b}$$

$$C_c = A_c + A_i + AB_q + B_i + B_c \tag{A.3c}$$

and

$$C_f = A_f + AB_k + AB_n + AB_r + B_f \tag{A.3d}$$

Equations relating C_d and C_e to their topologically similar diagrams are mirror images of (26a) and (26b) and provide no new information. The eight equations (A.2a–d) and (A.3a–d) enable us to completely determine the AB set by explicitly evaluating only a pair of AB diagrams. This provides enormous computational simplification not only in the determination of $\langle S^2\rangle_{app}$ but also in evaluating the

full structure factor $S(k)$ or the diffusion coefficient within the Kirkwood approximation.

Appendix B. Calculation of Diagrams

To determine all of the diagrams in the AB set, we must explicitly evaluate two of them; then the symmetry and topological relations described in section IIID can be employed to deduce the remaining eight. Equations A.3b and A.3d relate the sums $AB_o + AB_s$ and $AB_k + AB_n + AB_r$ to the simpler A, B, and C diagrams. By calculating AB_o (or AB_s) and AB_k (or AB_r) and using eq A.2a, we can immediately determine the other three members of these sums. Equations A.3a and A.3c provide AB_t and AB_q without recourse to any integrations of AB diagrams.

Following the rules for the interpretation of diagrams described in Section IIIA, diagram AB_k is

$$AB_k(\mathbf{c}_{21};N_A^0,N_B^0) = \int_0^{N_A^0 l_A} d\tau_2 \int_0^{\tau_2} d\tau_1 \int_0^{\tau_1} d\tau_A \int_0^{N_B^0 \tau_B} d\tau_B \int d\mathbf{c}_A(0) \int d\mathbf{c}_A(N_A^0) \int d\mathbf{c}_B(N_B^0) \int d\bar{\mathbf{c}}_1 \int d\bar{\mathbf{c}}_2\, \delta(\bar{\mathbf{c}}_1 - \bar{\mathbf{c}}_2) G_I^0(\bar{\mathbf{c}}_1 - \mathbf{c}_A(0);\tau_A) \times G_I^0(\mathbf{c}_1 - \bar{\mathbf{c}}_1;\tau_1 - \tau_A) G_I^0(\mathbf{c}_2 - \mathbf{c}_1;\tau_2 - \tau_1) \times G_I^0(\mathbf{c}_A(N_A^0) - \mathbf{c}_2;N_A^0 l_A - \tau_2) G_I^0(\bar{\mathbf{c}}_2 - \mathbf{c}_A(N_A^0);\tau_B) \times G_I^0(\mathbf{c}_B(N_B^0) - \bar{\mathbf{c}}_2;N_B^0 l_B - \tau_B) \quad \text{(B.1)}$$

It proves convenient to transform AB_k to its Fourier–Laplace representation according to

$$AB_k(\mathbf{q};s_A,s_B) = \int d\mathbf{c}_{21} \exp(i\mathbf{q}\cdot\mathbf{c}_{21}) \int_0^\infty d(N_A^0 l_A) \int_0^\infty d(N_B^0 l_B)\, AB_k(\mathbf{c}_{21};N_A^0,N_B^0) \quad \text{(B.2)}$$

Extensive use of the convolution theorem or of field theoretic methods discussed elsewhere[2] leads to

$$AB_k(\mathbf{q};s_A,s_B) = \frac{1}{s_A s_B} \int \frac{d\mathbf{P}}{(2\pi)^d} [\hat{G}_I^0(\mathbf{P};s_A)]^2 \hat{G}_I^0(\mathbf{P}-\mathbf{q};s_A) \hat{G}_I^0(\mathbf{P};s_B) \quad \text{(B.3)}$$

For $\delta\hat{G}_{AB}^0$ and $\delta\hat{G}_{AB}^{0\prime\prime}$ in eq 5, we require the $\mathbf{q} \to 0$ limits of eq B.3 and its d-dimensional Laplacian (see eq 6b). A pair of straightforward differentiations of the $\mathbf{q}$-dependent term under the integral sign followed by setting $\mathbf{q} = 0$ yields

$$AB_k''(s_A,s_B) = \frac{128}{s_A s_B} \int \frac{d\mathbf{P}}{(2\pi)^d} P^2 (P^2 + 2s_A)^{-5} (P^2 + 2s_B)^{-1} - \frac{32d}{s_A s_B} \int \frac{d\mathbf{P}}{(2\pi)^d} P^2 (P^2 + 2s_A)^{-4} (P^2 + 2s_B)^{-1} \quad \text{(B.4)}$$

while $AB_k(s_A,s_B)$ is

$$AB_k(s_A,s_B) = \frac{16}{s_A s_B} \int \frac{d\mathbf{P}}{(2\pi)^d} (P^2 + 2s_A)^{-3} (P^2 + 2s_B)^{-1} \quad \text{(B.5)}$$

We now outline the Laplace inversion of eq B.5. In general, any of the diagrams may be returned to $N_A^0 l_A$ and $N_B^0 l_B$ space by first using the identity[28]

$$\int \frac{d\mathbf{P}}{(2\pi)^d} \frac{P^{2l}}{(P^2 + 2s_A)^n (P^2 + 2s_B)^m} = \frac{1}{(2\pi)^{d/2}\Gamma(d/2) 2^{n+m-l}} \int_0^\infty \frac{d\chi\, \chi^{(d+2l-2)/2}}{(\chi + s_A)^n (\chi + s_B)^m} \quad \text{(B.6)}$$

Then, introduce 1 in the form

$$1 = \frac{\chi + s_i}{\chi} - \frac{s_i}{\chi}, \qquad i = A, B \quad \text{(B.7)}$$

into the integrands, followed by application of the inversion formulas

$$s_i^{-m} \int_0^\infty d\chi \frac{\chi^{(d-\beta-2)/2}}{(\chi + s_i)^n} \to [(N_i^0 l_i)^{n+m+(\beta/2)-3+(\epsilon/2)}] \frac{\Gamma\left(2 - \frac{\beta}{2} - \frac{\epsilon}{2}\right)\Gamma\left(n + \frac{\beta}{2} - 2 + \frac{\epsilon}{2}\right)}{\Gamma(n)\Gamma\left(n + m + \frac{\beta}{2} - 2 + \frac{\epsilon}{2}\right)} \quad \text{(B.8)}$$

or

$$\int_0^\infty \frac{d\chi\, \chi^{(d-\beta-2)/2}}{(\chi + s_A)^n (\chi + s_B)^m} \to \frac{(N_A^0 l_A)^{n-1} (N_B^0 l_B)^{m-1}}{\Gamma(n)\Gamma(m)} (N_A^0 l_A + N_B^0 l_B)^{(\beta/2)-2+(\epsilon/2)} \Gamma\left(2 - \frac{\beta}{2} - \frac{\epsilon}{2}\right) \quad \text{(B.9)}$$

After first applying eq B.6 to eq B.5, we have

$$AB_k(s_A,s_B) = \frac{1}{(2\pi)^{d/2}\Gamma(d/2) s_A s_B} \int_0^\infty \frac{d\chi\, \chi^{(d-2)/2}}{(\chi + s_A)^3 (\chi + s_B)}$$

several iterations of (B.7) are necessary to put AB_k in the easily inverted form

$$AB_k(s_A,s_B) = \frac{1}{(2\pi)^{d/2}\Gamma(d/2)} \left[\frac{1}{s_A s_B} \int_0^\infty \frac{d\chi\, \chi^{(d-4)/2}}{(\chi + s_A)^3} - \frac{1}{s_A} \int_0^\infty \frac{d\chi\, \chi^{(d-10)/2}}{(\chi + s_B)} + \int_0^\infty \frac{d\chi\, \chi^{(d-10)/2}}{(\chi + s_A)(\chi + s_B)} + \int_0^\infty \frac{d\chi\, \chi^{(d-8)/2}}{(\chi + s_A)^2 (\chi + s_B)} + \int_0^\infty \frac{d\chi\, \chi^{(d-6)/2}}{(\chi + s_A)^3 (\chi + s_B)} \right]$$

which becomes

$$AB_k(N_A^0,N_B^0) = \frac{(N_A^0 l_A + N_B^0 l_B)^{2+\epsilon/2}}{(2\pi)^{d/2}\Gamma(d/2)} \left\{ x_A^{0\,2+\epsilon/2} \Gamma(1 - \epsilon/2)\Gamma(2 + \epsilon/2)[2\Gamma(3 + \epsilon/2)]^{-1} + [1 - x_B^{0\,2+\epsilon/2}]\Gamma\left(-2 - \frac{\epsilon}{2}\right) + x_A^0 \Gamma(-1 - \epsilon/2) + \left(\frac{x_A^{0\,2}}{2}\right)\Gamma\left(-\frac{\epsilon}{2}\right) \right\} \quad \text{(B.10)}$$

upon inversion.

The inversion of $AB_k''(s_A,s_B)$ is even more tedious but follows the same procedure giving the result

$$AB_k''(N_A^0,N_B^0) = \frac{(N_A^0 l_A + N_B^0 l_B)^{3+\epsilon/2}}{(2\pi)^{d/2}\Gamma(d/2)} \left\{ (4 - d) \times \left[\frac{(1 - \epsilon/2)\Gamma(3 + \epsilon/2)}{6\Gamma(4 + \epsilon/2)} x_A^{0\,3+\epsilon/2} + (1 - x_B^{0\,3+\epsilon/2})\Gamma(-3 - \epsilon/2) + x_A^0 \Gamma(-2 - \epsilon/2) + \left(\frac{x_A^{0\,2}}{2}\right)\Gamma(-1 - \epsilon/2) + \left(\frac{x_A^{0\,3}}{6}\right)\Gamma\left(-\frac{\epsilon}{2}\right) \right] + \left(\frac{1}{6}\right) x_A^{0\,3} (x_A^0 - x_A^{0\,\epsilon/2})\Gamma(1 - \epsilon/2) \right\} \quad \text{(B.11)}$$

AB_r and AB_r'' are obtained from (B.10) and (B.11) by reversing the A and B subscripts. Similarly, AB_o and AB_o'' are

$$AB_o(N_A^0,N_B^0) = \frac{(N_A^0 l_A + N_B^0 l_B)^{2+(\epsilon/2)}}{(2\pi)^{1/2}\Gamma\left(\frac{d}{2}\right)}\Bigg[\Gamma\left(1 - \frac{\epsilon}{2}\right)\Gamma\left(1 + \frac{\epsilon}{2}\right)x_A^{0^{1+\epsilon/2}}x_B^0/\Gamma(2+\epsilon/2) - \Gamma(-\epsilon/2)\Gamma(2+\epsilon/2)x_A^{0^{2+\epsilon/2}}[\Gamma(3+\epsilon/2)]^{-1} + \Gamma(-2-\epsilon/2)(x_B^{0^{2+\epsilon/2}} - 1) - x_A^0\Gamma(-1-\epsilon/2)\Bigg] \quad \text{(B.12)}$$

and

$$AB_o''(N_A^0,N_B^0) = \frac{(N_A^0 l_A + N_B^0 l_B)^{3+(\epsilon/2)}}{(2\pi)^{d/2}\Gamma(d/2)}\Bigg\{2\Gamma(2-\epsilon/2)\times\Gamma(2+\epsilon/2)x_A^{0^{2+\epsilon/2}}x_B^0/[3\Gamma(3+\epsilon/2)] - 2\Gamma(1-\epsilon/2)\Gamma(3+\epsilon/2)x_A^{0^{3+\epsilon/2}}/[3\Gamma(4+\epsilon/2)] + 4(x_B^{0^{3+\epsilon/2}} - 1)\Gamma\left(-3 - \frac{\epsilon}{2}\right) - 4x_A^0\Gamma(-2-\epsilon/2) + \left(\frac{d}{2} - 2\right)x_A^{0^2}\Gamma(-1-\epsilon/2) - \frac{2}{3}x_A^{0^3}\Gamma(-\epsilon/2) - dx_A^{0^{2+\epsilon/2}}\frac{\Gamma(1-\epsilon/2)\Gamma(2+\epsilon/2)}{2\Gamma(3+\epsilon/2)} + dx_A^{0^{3+\epsilon/2}}\Gamma\left(-\frac{\epsilon}{2}\right)\Gamma\left(3+\frac{\epsilon}{2}\right)\Big/[2\Gamma(4+\epsilon/2)] - dx_A^{0^{1+\epsilon/2}}\Gamma(1-\epsilon/2)\Gamma(1+\epsilon/2)/[2\Gamma(2+\epsilon/2)] + dx_A^{0^{2+\epsilon/2}}\Gamma(-\epsilon/2)\Gamma(2+\epsilon/2)/\Gamma(3+\epsilon/2) - dx_A^{0^{3+\epsilon/2}}\Gamma(-1-\epsilon/2)\Gamma(3+\epsilon/2)/\Gamma(4+\epsilon/2)\Bigg\} \quad \text{(B.13)}$$

The symmetry and topological relations we derive in Appendix A hold for the diagrams in Fourier space as well as for the original $\mathbf{c}_{21}$-dependent quantities. We can also compare the ϵ expansions of both sides of eq A.2a–d and A.2a–d to obtain AB diagrams to any desired order of ϵ. The point at which the symmetry and topological arguments are used to derive the remaining AB diagrams is a matter of convenience. Finally, we note that the A, B, and C diagrams can be evaluated along exactly the same lines as outlined for the AB ones. We omit the details except to note that powers of $(2s_A + P^2)^{-1}$ or $(2s_B + P^2)^{-1}$—but not both—occur in the integrands of the Laplace-transformed diagrams making their evaluation far less difficult than the calculations summarized in this Appendix.

References and Notes

(1) Freed, K. F. *Acc. Chem. Res.* **1985**, *18*, 38.
(2) Freed, K. F. *Renormalization Group Theory of Macromolecules*; Wiley: New York, 1987.
(3) (a) Edwards, S. F. *Proc. Phys. Soc. London* **1975**, *88*, 265. (b) *J. Phys. A* **1975**, *10*, 1670.
(4) Ohta, T.; Oono, Y. *Phys. Lett. A* **1982**, *89*, 460.
(5) (a) Ohta, T.; Oono, Y.; Freed, K. F. *Phys. Rev. A* **1982**, *25*, 2801. (b) Witten, T. A., Jr.; Schäfer, L. *J. Chem. Phys.* **1981**, *74*, 2582.
(6) Douglas, J. F.; Freed, K. F. *Macromolecules* **1984**, *17*, 1854.
(7) (a) Freed, K. F.; Douglas, J. F. *J. Chem. Phys.* **1988**, *88*, 2764. (b) Muthukumar, M.; Nickel, B. G. *J. Chem. Phys.* **1984**, *80*, 5839. (c) Douglas, J. F.; Freed, K. F. *Macromolecules* **1984**, *17*, 2344; **1985**, *18*, 201.
(8) (a) Edwards, S. F. *Proc. Phys. Soc.* **1965**, *85*, 613; (b) **1986**, *88*, 265.
(9) (a) Yamakawa, H. *Modern Theory of Polymer Solutions*; Harper and Row: New York, 1971. (b) Zimm, B. H.; Stockmayer, W. H.; Fixman, M. *J. Chem. Phys.* **1953**, *21*, 1716. (c) Fixman, M. *Ibid.* **1955**, *23*, 1656. (d) Stockmayer, W. H. *Makromol. Chem.* **1960**, *35*, 54.
(10) (a) Oono, Y.; Kohmoto, M. *J. Chem. Phys.* **1983**, *78*, 520. (b) Oono, Y. *J. Chem. Phys.* **1983**, *79*, 4629. (c) Jasnow, D.; Moore, M. A. *J. Phys. (Paris)* **1978**, *38*, 2467. (d) Wang, S.-Q.; Douglas, J. F.; Freed, K. F. *Macromolecules* **1985**, *18*, 2464; *J. Chem. Phys.* **1986**, *85*, 3674.
(11) Kirkwood, J. G.; Riseman, J. *J. Chem. Phys.* **1948**, *16*, 565.
(12) (a) Tanaka, T.; Kotaka, T.; Inagaki, H. *Macromolecules* **1976**, *9*, 561. (b) Tanaka, T.; Kotaka, T.; Ban, K.; Hattori, M.; Inagaki, H. *Ibid.* **1977**, *10*, 960. (c) Tanaka, T.; Omoto, M.; Inagaki, H. *Macromolecules* **1979**, *12*, 146. (d) Fukuda, T.; Inagaki, H. *Pure Appl. Chem.* **1983**, *55*, 1541. (e) Tanaka, T.; Inagaki, H. *Polym. Prepr. (Am. Chem. Soc., Div. Polym. Chem.)* **1979**, *20*, 9.
(13) Douglas, J. F.; Freed, K. F. *J. Chem. Phys.* **1987**, *86*, 4280. Note that eq 4.25a contains a typographical error and should have $768[(1 - x^0)/x^0]^{7/2}$ instead of $768[(1 - x^0)/x^0]^{7/2}$.
(14) (a) Joanny, J.; Leibler, L.; Ball, R. *J. Chem. Phys.* **1984**, *81*, 4640. (b) Kosmas, M. K. *J. Phys.* **1984**, *45*, L-889. (c) Soranis, Y. S.; Kosmas, M. K. *J. Chem. Soc., Faraday Trans. 2* **1987**, *83*, 819.
(15) (a) Gaylor, N. In *Copolymer, Polyblends and Composites*; Platzer, N., Ed.; American Chemical Society: Washington, DC, 1975; p 75. (b) Cantor, R. *Macromolecules* **1981**, *14*, 1186. (c) Krause, J. S. *J. Macromol. Sci. Rev. Macromol. Chem. C* **1972**, *7*, 251. (d) Fayt, R.; Jérome, J.; Teyssié, P. *J. Polym. Sci.* **1982**, *20*, 2209. (e) Meier, D. J. *J. Polym. Sci. C* **1969**, *26*, 81.
(16) Benoit, H.; Fröelich, D. In *Light Scattering from Polymer Solutions*; Huglin, M. B., Ed.; Academic Press: London, 1972.
(17) Fröelich, P. D.; Bnoit, H. *Makromol. Chem.* **1966**, *92*, 24.
(18) Yamakawa, H.; Kurata, M. *J. Chem. Phys.* **1960**, *32*, 1852.
(19) Sato, H.; Kamada, K. *Bull. Chem. Soc. Jpn.* **1967**, *40*, 2264.
(20) Sikora, A. *Makromol. Chem.* **1978**, *179*, 633.
(21) Edwards, S. F. *J. Phys. A* **1974**, *7*, 332. The scaling we employ to eliminate factors of l_A, l_B, and d in the Hamiltonian (see eq 1) differs from that used in previous treatments of homopolymers where $\mathbf{c} = (d/l)^{1/2}\mathbf{r}$ and the upper limits on the contour variables, the τ's, do not contain l.
(22) The presence of different blocks with separate temperature and solvent quality dependence suggests the need for two phenomenological length scales, L_A and L_B. However, as noted in ref 13, a single L suffices to describe the diblock properties in terms of three phenomenological excluded-volume parameters.
(23) We employ the method of dimensional regularization which avoids the need for explicit cutoffs in the calculations. Instead, singularities in ϵ arise in the bare (or unrenormalized) results which are systematically removed upon replacing the bare quantities by their renormalized counterparts. See ref 2 and: Gell-Mann, M.; Low, F. E. *Phys. Rev.* **1954**, *95*, 1300. 't Hooft, G.; Veltman, M. *Nucle. Phys. B* **1972**, *44*, 189.
(24) Cherayil, B. C.; Freed, K. F. *J. Chem. Phys.* **1988**, *88*, 7851.
(25) Wall, F. T.; Erpenbeck, J. J. *J. Chem. Phys.* **1959**, *30*, 634.
(26) The relationship of our $\bar{z}_A$, $\bar{z}_B$, and $\bar{z}_{AB}$ variables to the (quite different) interaction parameters used in the simulations is complicated, so a quantitative comparison of our theory to the Monte Carlo results is not easily accomplished.
(27) (a) Douglas, J. F.; Nemirovsky, A. M.; Freed, K. F. *Macromolecules* **1986**, *19*, 2041. (b) Douglas, J. F.;: Wang, S. Q.; Freed, K. F. *Macromolecules* **1987**, *20*, 543.
(28) Ramond, P. *Field Theory, A Modern Primer*; Benjamin/Cummings: Reading, MA, 1981.